Coralie Germain
Institut de Recherche en Communications
et Cybernétique de Nantes IRCCyN,
UMR CNRS 6597,
1, rue de la Noë,
Nantes 44321, France
e-mail: coralie.germain@ens-rennes.fr

Sébastien Briot[1]
Institut de Recherche en Communications
et Cybernétique de Nantes IRCCyN,
UMR CNRS 6597,
1, rue de la Noë,
Nantes 44321, France
e-mail: Sebastien.Briot@irccyn.ec-nantes.fr

Stéphane Caro
Institut de Recherche en Communications
et Cybernétique de Nantes IRCCyN,
UMR CNRS 6597,
1, rue de la Noë,
Nantes 44321, France
e-mail: Stephane.Caro@irccyn.ec-nantes.fr

Philippe Wenger
Institut de Recherche en Communications
et Cybernétique de Nantes IRCCyN,
UMR CNRS 6597,
1, rue de la Noë,
Nantes 44321, France
e-mail: Philippe.Wenger@irccyn.ec-nantes.fr

Natural Frequency Computation of Parallel Robots

The characterization of the elastodynamic behavior and natural frequencies of parallel robots is a crucial point. Accurate elastodynamic models of parallel robots are useful at both their design and control stages in order to define their optimal dimensions and shapes while improving their vibratory behavior. Several methods exist to write the elastodynamic model of manipulators. However, those methods do not provide a straightforward way to write the Jacobian matrices related to the kinematic constraints of parallel manipulators. Therefore, the subject of this paper is about a systematic method for the determination of the mass and stiffness matrices of any parallel robot in stationary configurations. The proposed method is used to express the mass and stiffness matrices of the Nantes Variable Actuation Robot (NaVARo), a three-degree-of-freedom (3DOF) planar parallel robot with variable actuation schemes, developed at IRCCyN. Then, its natural frequencies are evaluated and compared with those obtained from both CAST3M *software and experimentally*. [DOI: 10.1115/1.4028573]

1 Introduction

Parallel robots have been increasingly used in industry in the last few years for pick-and-place applications and high-speed machining [1,2]. This interest is mainly due to their high stiffness and good dynamic performance compared with their serial manipulator counterparts.

Having a good knowledge of the elastodynamic behavior of a manipulator (especially its natural frequencies) is a crucial point. As a consequence, accurate elastodynamic models of parallel robots are useful at both their design [3–5] and control [6–8] stages in order to define their optimal dimensions and shapes while improving their vibratory behavior.

Several models have been proposed and used in order to compute the natural frequencies of a mechanism. For instance, the following three methods are commonly used in the literature:

- Finite element analysis (FEA): The FEA method is proved to be the most accurate and reliable, since the links and joints are modeled with their true dimensions and shape [9,10]. However, its accuracy is limited by the mesh size and is usually used at the final design stage of the robot because the meshing is time consuming.
- Matrix structural analysis (MSA) method is a common technique in mechanical engineering [4,11–14]. It incorporates the main ideas of the FEA method but operates with rather large flexible elements (beams, arcs, cables, and so on). As a result, the MSA method is less time consuming than the FEA method, but requires good knowledge in FEA.
- Virtual joint method (VJM) [5,15], which is also referred to as "lumped modeling," is based on the expansion of the traditional rigid model by adding virtual joints (localized springs), which describe the elastic deformations of the manipulator components (links, joints, and actuators). Lumped modeling is simpler to use but is less accurate than MSA.

Some general methodologies dealing with MSA or VJM are presented in Refs. [11–13,15]. These methodologies can differ from the type of elements or flexible models used. Nevertheless, all of them require the determination of some Jacobian matrices in order to characterize kinematic dependencies in closed-loop mechanisms. The main drawback of such methodologies is that they are not specifically designed for parallel robots and they do not propose a systematic and straightforward way for computing the Jacobian matrices required for closing the loops.

An approach for the systematic computation of these matrices was proposed in Ref. [4]. However, this approach is complicated and the obtained results have been verified neither with a commercial software nor experimental. In Ref. [14], the authors proposed an interesting algorithm to study the elastodynamic behavior of parallel robots that considers both the joint and link flexibilities. The way the authors close the robot loops and choose the independant coordinates is not straightforward, resulting in a potentially asymmetrical description of the leg variables.

This paper aims at developing a simple and straightforward procedure for the computation of mass and stiffness matrices of parallel robots in stationary configurations. Indeed,

- a simple way to compute the Jacobian matrices required for closing the robot loops is presented, and
- the set of independent coordinates for parallel robots with a symmetrical arrangement are chosen cleverly.

The judicious choice of the set of independent coordinates for parallel robots with a symmetrical arrangement aims at

[1]Corresponding author.

Contributed by the Design Engineering Division of ASME for publication in the JOURNAL OF COMPUTATIONAL AND NONLINEAR DYNAMICS. Manuscript received July 30, 2013; final manuscript received September 11, 2014; published online January 12, 2015. Assoc. Editor: Arend L. Schwab.

simplifying the robot elastodynamic modeling and the comprehension of the robot behavior for each natural frequency. Symmetry is kept in the variable description in order to have the same information on the evolution of the same variables for robots having legs with the same kinematic chains.

Moreover, contrary to most of the existing methods, the proposed approach does not contain any numerical matrix inversion, which is better to avoid numerical issues that may lead to a loss in the result accuracy. The natural frequencies calculated using this procedure will be compared with simulation data obtained using an FEA/MSA software and with experiments carried out on a parallel robot.

A methodology similar to the one presented in Ref. [16] to obtain the *rigid dynamic model* of a parallel robot is used. For a parallel robot composed of rigid or flexible links connected by passive or active joints, such as the one described in Fig. 1, the methodology is decomposed into two steps:

(1) All closed-loops are virtually opened in such a way that the platform is virtually disassembled from the robot architecture (Fig. 1(*b*)). Each joint is virtually considered actuated so that the robot becomes a tree structure with a free body: the platform. The mass and stiffness matrices of the tree structure and the ones of the free platform are then computed.
(2) The loops are closed using Jacobian matrices so that the mass and stiffness matrices of the actual parallel robot can be obtained.

The paper is organized as follows. In Sec. 2, a method used for the computation of the mass and stiffness matrices of one single flexible body using MSA techniques is recalled. The mass and stiffness matrices of the virtual system composed of the tree structure and the free platform are introduced in Sec. 3. A straightforward way for the computation of the Jacobian matrices linking the Cartesian coordinates of each body to the generalized coordinates of the virtual system is proposed. Section 4 describes the proposed method to close the loops in order to obtain the mass and stiffness matrices of the actual parallel robot that keeps a symmetrical description of the leg variables. The natural frequencies of the NaVARo [17,18] are then evaluated in Sec. 5. NaVARo is a 3DOF planar parallel manipulator with multiple actuation modes developed at IRCCyN. Moreover, the simulation results obtained with our approach are compared with both CAST3M software [19] and experiments. Finally, Sec. 6 concludes this paper.

2 Computation of the Stiffness and Mass Matrices of a Flexible Body

2.1 Kinematics of a Flexible Free Body. Let us consider body j described in Fig. 2(*a*) to which a local frame $\mathcal{F}_j$ is attached at point A_j. The flexible body is considered as the superposition of the undeformed configuration referred to as 0, which corresponds to a rigid transformation of body j described by variable q_j and the deformed configuration related to the elastic deformation of the body. The translational velocity of any material point M_j of this flexible body can be expressed as [20]

$$\mathbf{v}_j(M_j) = \mathbf{v}_j(A_j) + \boldsymbol{\omega}_j(A_j) \times \mathbf{r}_j(M_j) + \mathbf{v}_{\mathrm{e}_j}(M_j) \tag{1}$$

where $\mathrm{v}_j(A_j)$ and $\boldsymbol{\omega}_j(A_j)$ are the translational and rotational velocities of body j expressed in frame $\mathcal{F}_j$, respectively, $\mathbf{r}_j(M_j)$ is the position vector of point M_j (of the deformed body) expressed in frame $\mathcal{F}_j$, $\mathbf{v}_{\mathrm{e}_j}(M_j)$ is the translational velocity due to the body elasticity that can be parameterized as truncated series of Rayleigh–Ritz shape functions

$$\mathbf{v}_{\mathrm{e}_j}(M_j) = \boldsymbol{\Phi}_{\mathrm{d}_j}(M_{0j})\dot{\mathbf{q}}_{\mathrm{e}_j} \tag{2}$$

with $\boldsymbol{\Phi}_{\mathrm{d}_j} = \left[\boldsymbol{\phi}_{\mathrm{d}1_j} \cdots \boldsymbol{\phi}_{dN_jj}\right]$ of size $(3 \times N_j)$, $\boldsymbol{\phi}_{\mathrm{d}k_j}(M_{0j})$ being a three-dimensional vector (3D) containing the kth shape functions for the displacement of the flexible body at point M_{0j}, and $\dot{\mathbf{q}}_{\mathrm{e}_j} = \left[\dot{q}_{\mathrm{e}1_j} \cdots \dot{q}_{\mathrm{e}N_jj}\right]^{\mathrm{T}}$, $\dot{q}_{\mathrm{e}k_j}$ being the kth elastic generalized velocity of body j and N_j the number of considered shape functions. It should be noted that vector $\mathbf{r}_j(M_j)$ in Eq. (1) can be expressed as

$$\mathbf{r}_j(M_j) = \mathbf{r}_j(M_{0j}) + \mathbf{u}_{\mathrm{e}_j}(M_{0j}) \tag{3}$$

where $\mathbf{r}_j(M_{0_j})$ is the position vector of point M_{0j} expressed in frame $\mathcal{F}_j$

$$\mathbf{u}_{\mathrm{e}_j}(M_{0j}) = \boldsymbol{\Phi}_{\mathrm{d}_j}(M_{0j})\mathbf{q}_{\mathrm{e}_j} \tag{4}$$

is the elastic displacement that transforms M_{0j} to M_j and $\mathbf{q}_{\mathrm{e}_j} = \left[q_{\mathrm{e}1_j} \cdots q_{\mathrm{e}N_jj}\right]^{\mathrm{T}}$ is the vector of elastic generalized coordinates of body j.

Equation (1) can thus be written in the following matrix form:

$$\mathbf{v}_j(M_j) = \begin{bmatrix} \mathbf{I}_3 & \left[\mathbf{r}_j(M_j)\right]_{\times}^{\mathrm{T}} & \boldsymbol{\Phi}_{\mathrm{d}_j}(M_{0j}) \end{bmatrix} \begin{bmatrix} \mathbf{v}_j(A_j) \\ \boldsymbol{\omega}_j(A_j) \\ \dot{\mathbf{q}}_{\mathrm{e}_j} \end{bmatrix} \tag{5}$$

where $\mathbf{I}_3$ is the (3×3) identity matrix and $[\mathbf{r}_j(M_j)]_{\times}$ is the cross-product matrix of vector $\mathbf{r}_j(M_j)$.

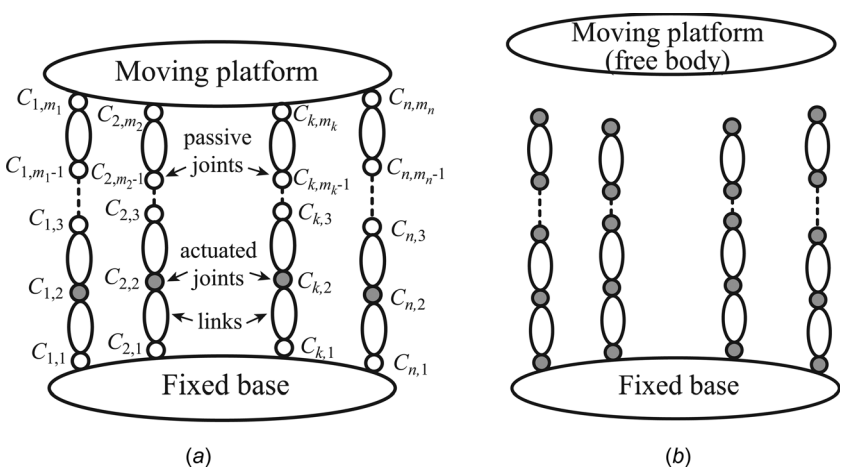

Fig. 1 Schematic of a parallel robot for its dynamic modeling: (*a*) kinematic chain and (*b*) virtual tree structure

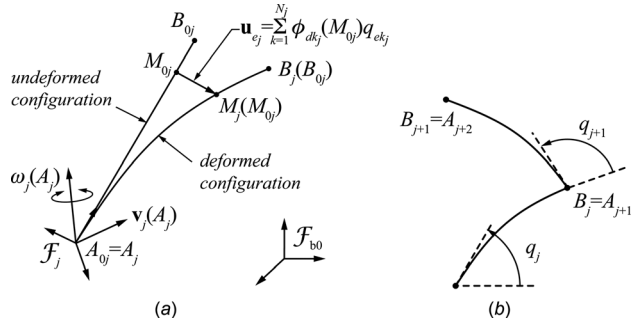

Fig. 2 Schematics of the flexible elements into consideration: (*a*) parameters of one flexible body *j* and (*b*) assembly of two flexible bodies

Equations (1)–(5) define the kinematic model of flexible free body j. This model is thus parameterized by the following set of variables:

- $\mathbf{v}_j(A_j)$ and $\boldsymbol{\omega}_j(A_j)$: Cartesian velocities (Euler variables) characterizing the rigid displacement of body j expressed in frame $\mathcal{F}_j$;
- $\mathbf{q}_{e_j}$: generalized coordinates (Lagrange variables) characterizing the elastic displacements of body j.

It should be mentioned that this description can be applied to both robot links and joints, as long as all the shape functions can be defined.

2.2 Kinetic Energy of a Flexible Free Body. The kinetic energy of body j (denoted as Σ_j in the following integral) is given by:

$$T_j = \frac{1}{2}\int_{\Sigma_j} \mathbf{v}_j(M_j)^{\mathrm{T}}\mathbf{v}_j(M_j)\mathrm{dm} = \frac{\rho_j}{2}\int_{V_j} \mathbf{v}_j(M_j)^{\mathrm{T}}\mathbf{v}_j(M_j)\mathrm{dV} \tag{6}$$

where ρ_j is the material density and V_j is the body volume.

Introducing Eq. (5) into Eq. (6) leads to

$$T_j = \frac{\rho_j}{2}\int_{V_j} \begin{bmatrix} \mathbf{v}_j(A_j) \\ \boldsymbol{\omega}_j(A_j) \\ \dot{\mathbf{q}}_{e_j} \end{bmatrix}^{\mathrm{T}} \begin{bmatrix} \mathbf{I}_3 \\ [\mathbf{r}_j(M_j)]_\times \\ \boldsymbol{\Phi}_{d_j}(M_{0j})^{\mathrm{T}} \end{bmatrix} \begin{bmatrix} \mathbf{I}_3 & [\mathbf{r}_j(M_j)]_\times^{\mathrm{T}} & \boldsymbol{\Phi}_{d_j}(M_{0j}) \end{bmatrix} \times \begin{bmatrix} \mathbf{v}_j(A_j) \\ \boldsymbol{\omega}_j(A_j) \\ \dot{\mathbf{q}}_{e_j} \end{bmatrix} \mathrm{dV} = \frac{1}{2}\begin{bmatrix} \mathbf{v}_j(A_j) \\ \boldsymbol{\omega}_j(A_j) \\ \dot{\mathbf{q}}_{e_j} \end{bmatrix}^{\mathrm{T}} \mathbf{M}_j \begin{bmatrix} \mathbf{v}_j(A_j) \\ \boldsymbol{\omega}_j(A_j) \\ \dot{\mathbf{q}}_{e_j} \end{bmatrix} \tag{7}$$

where

$$\mathbf{M}_j = \rho_j \int_{V_j} \begin{bmatrix} \mathbf{I}_3 & [\mathbf{r}_j(M_j)]_\times^{\mathrm{T}} & \boldsymbol{\Phi}_{d_j}(M_{0j}) \\ [\mathbf{r}_j(M_j)]_\times & [\mathbf{r}_j(M_j)]_\times[\mathbf{r}_j(M_j)]_\times^{\mathrm{T}} & [\mathbf{r}_j(M_j)]_\times\boldsymbol{\Phi}_{d_j}(M_{0j}) \\ \boldsymbol{\Phi}_{d_j}(M_{0j})^{\mathrm{T}} & \boldsymbol{\Phi}_{d_j}(M_{0j})^{\mathrm{T}}[\mathbf{r}_j(M_j)]_\times^{\mathrm{T}} & \boldsymbol{\Phi}_{d_j}(M_{0j})^{\mathrm{T}}\boldsymbol{\Phi}_{d_j}(M_{0j}) \end{bmatrix} \mathrm{dV} \tag{8}$$

$\mathbf{M}_j$ is the mass matrix of body j expressed in its frame $\mathcal{F}_j$.

2.3 Elastic Potential Energy and Stiffness Matrix of a Flexible Free Body. The elastic potential energy of any body is given by Shabana [11]

$$V_{e_j} = \frac{1}{2}\int_{V_j} \boldsymbol{\sigma}_j^{\mathrm{T}}\mathbf{I}_{\mathrm{t}}\boldsymbol{\epsilon}_j\mathrm{dV} \tag{9}$$

where $\boldsymbol{\sigma}_j$ and $\boldsymbol{\epsilon}_j$ are the six-dimensional stress and strain vectors due to the small elastic displacement $\mathbf{u}_{e_j}(M_{0j})$ in body j. $\mathbf{I}_{\mathrm{t}}$ is a (6×6) diagonal matrix. The first three diagonal terms are equal to one, whereas the last three diagonal terms are equal to two, because of the two multipliers associated with the shear strains [11]. The strain vector is defined as $\boldsymbol{\epsilon}_j = [\,\epsilon_{j11} \quad \epsilon_{j22} \quad \epsilon_{j33} \quad \epsilon_{j12} \quad \epsilon_{j13} \quad \epsilon_{j23}\,]^{\mathrm{T}}$, where

$$\begin{bmatrix} \epsilon_{j11} & \epsilon_{j12} & \epsilon_{j13} \\ \epsilon_{j12} & \epsilon_{j22} & \epsilon_{j23} \\ \epsilon_{j13} & \epsilon_{j23} & \epsilon_{j33} \end{bmatrix} = \frac{1}{2}\left(\nabla\mathbf{u}_{e_j}(M_{0j}) + \left(\nabla\mathbf{u}_{e_j}(M_{0j})\right)^{\mathrm{T}}\right) \tag{10}$$

with

$$\nabla\mathbf{u}_{e_j}(M_{0j}) = \begin{bmatrix} \dfrac{\partial\mathbf{u}_{e_j}}{\partial x}(M_{0j}) & \dfrac{\partial\mathbf{u}_{e_j}}{\partial y}(M_{0j}) & \dfrac{\partial\mathbf{u}_{e_j}}{\partial z}(M_{0j}) \end{bmatrix} = \begin{bmatrix} \dfrac{\partial\boldsymbol{\Phi}^1_{d_j}}{\partial x}(M_{0j})\mathbf{q}_{e_j} & \dfrac{\partial\boldsymbol{\Phi}^1_{d_j}}{\partial y}(M_{0j})\mathbf{q}_{e_j} & \dfrac{\partial\boldsymbol{\Phi}^1_{d_j}}{\partial z}(M_{0j})\mathbf{q}_{e_j} \\ \dfrac{\partial\boldsymbol{\Phi}^2_{d_j}}{\partial x}(M_{0j})\mathbf{q}_{e_j} & \dfrac{\partial\boldsymbol{\Phi}^2_{d_j}}{\partial y}(M_{0j})\mathbf{q}_{e_j} & \dfrac{\partial\boldsymbol{\Phi}^2_{d_j}}{\partial z}(M_{0j})\mathbf{q}_{e_j} \\ \dfrac{\partial\boldsymbol{\Phi}^3_{d_j}}{\partial x}(M_{0j})\mathbf{q}_{e_j} & \dfrac{\partial\boldsymbol{\Phi}^3_{d_j}}{\partial y}(M_{0j})\mathbf{q}_{e_j} & \dfrac{\partial\boldsymbol{\Phi}^3_{d_j}}{\partial z}(M_{0j})\mathbf{q}_{e_j} \end{bmatrix} \tag{11}$$

where $\boldsymbol{\Phi}^k_{d_j}$ corresponds to the kth line of matrix $\boldsymbol{\Phi}_{d_j}, k = 1,2,3$. As a result

$$\boldsymbol{\epsilon}_j = \begin{bmatrix} \dfrac{\partial\boldsymbol{\Phi}^1_{d_j}}{\partial x}(M_{0j}) \\ \dfrac{\partial\boldsymbol{\Phi}^2_{d_j}}{\partial y}(M_{0j}) \\ \dfrac{\partial\boldsymbol{\Phi}^3_{d_j}}{\partial z}(M_{0j}) \\ \dfrac{1}{2}\left(\dfrac{\partial\boldsymbol{\Phi}^1_{d_j}}{\partial y}(M_{0j}) + \dfrac{\partial\boldsymbol{\Phi}^2_{d_j}}{\partial x}(M_{0j})\right) \\ \dfrac{1}{2}\left(\dfrac{\partial\boldsymbol{\Phi}^1_{d_j}}{\partial z}(M_{0j}) + \dfrac{\partial\boldsymbol{\Phi}^3_{d_j}}{\partial x}(M_{0j})\right) \\ \dfrac{1}{2}\left(\dfrac{\partial\boldsymbol{\Phi}^2_{d_j}}{\partial z}(M_{0j}) + \dfrac{\partial\boldsymbol{\Phi}^3_{d_j}}{\partial y}(M_{0j})\right) \end{bmatrix}\mathbf{q}_{e_j} = \boldsymbol{\Phi}_{\epsilon_j}\mathbf{q}_{e_j} \tag{12}$$

The stress vector is expressed as

$$\boldsymbol{\sigma}_j = [\,\sigma_{j11} \quad \sigma_{j22} \quad \sigma_{j33} \quad \sigma_{j12} \quad \sigma_{j13} \quad \sigma_{j23}\,]^{\mathrm{T}} = \mathbf{E}_j\boldsymbol{\epsilon}_j \tag{13}$$

where matrix $\mathbf{E}_j$ is given by the Hooke's law [11].

Thus, introducing Eqs. (12) and (13) into Eq. (9) leads to

$$V_{e_j} = \frac{1}{2}\mathbf{q}_{e_j}^{\mathrm{T}}\mathbf{K}_j\mathbf{q}_{e_j} \tag{14}$$

where $\mathbf{K}_j$ is the stiffness matrix of body j and takes the form

$$\mathbf{K}_j = \int_{V_j} \mathbf{\Phi}_{\epsilon_j}^{\mathrm{T}} \mathbf{E}_j^{\mathrm{T}} \mathbf{I}_t \mathbf{\Phi}_{\epsilon_j} \mathrm{dV} \tag{15}$$

2.4 Case of the Elastic Beam: The Bernoulli Model. The computation of the mass and stiffness matrices of 3D beams is useful for the elastodynamic modeling of parallel manipulators.

The Bernoulli model describes the beam deformation under the assumption that the shear effect is negligible, that the cross sections remain perpendicular to the neutral axis and that the rotational inertia of sections is assumed to be zero [21]. With such a model, the 3D beam deformation $\mathbf{u}_{\epsilon_j}(M_{0j})$ (see Sec. 2.1) can be characterized with the six shape functions $\phi_{\mathrm{dx}_j}, \phi_{\mathrm{dy}_j}, \phi_{\mathrm{dz}_j}, \phi_{\mathrm{rx}_j}, \phi_{\mathrm{ry}_j}$, and ϕ_{rz_j}, i.e., $N_j = 6$, defined as

$$\boldsymbol{\phi}_{\mathrm{dx}_j} = \begin{bmatrix} \xi & 0 & 0 & 0 & 0 & 0 \end{bmatrix} \tag{16a}$$

$$\boldsymbol{\phi}_{\mathrm{dy}_j} = \begin{bmatrix} 0 & 3\xi^2 - 2\xi^3 & 0 & 0 & 0 & l_j(\xi^3 - \xi^2) \end{bmatrix} \tag{16b}$$

$$\boldsymbol{\phi}_{\mathrm{dz}_j} = \begin{bmatrix} 0 & 0 & 3\xi^2 - 2\xi^3 & 0 & -l_j(\xi^3 - \xi^2) & 0 \end{bmatrix} \tag{16c}$$

$$\boldsymbol{\phi}_{\mathrm{rx}_j} = \begin{bmatrix} 0 & 0 & 0 & \xi & 0 & 0 \end{bmatrix} \tag{16d}$$

$$\boldsymbol{\phi}_{\mathrm{ry}_j} = \begin{bmatrix} 0 & 0 & -6(\xi - \xi^2)/l_j & 0 & 3\xi^2 - 2\xi & 0 \end{bmatrix} \tag{16e}$$

$$\boldsymbol{\phi}_{\mathrm{rz}_j} = \begin{bmatrix} 0 & 6(\xi - \xi^2)/l_j & 0 & 0 & 0 & 3\xi^2 - 2\xi \end{bmatrix} \tag{16f}$$

where $\xi = x/l_j$ and l_j is the beam length.

x, y, and z denote the Cartesian coordinates of point M_{0j} expressed in the local frame $\mathcal{F}_j$ and $\mathbf{\Phi}_{\mathrm{d}_j}(M_{0j})$ is a (3×6) matrix that takes the form

$$\mathbf{\Phi}_{\mathrm{d}_j}(M_{0j}) = \begin{bmatrix} \boldsymbol{\phi}_{\mathrm{dx}_j} - y\boldsymbol{\phi}_{\mathrm{rz}_j} + z\boldsymbol{\phi}_{\mathrm{ry}_j} \\ \boldsymbol{\phi}_{\mathrm{dy}_j} - z\boldsymbol{\phi}_{\mathrm{rx}_j} \\ \boldsymbol{\phi}_{\mathrm{dz}_j} + y\boldsymbol{\phi}_{\mathrm{rx}_j} \end{bmatrix} \tag{17}$$

Moreover, in the beam model, it is assumed that

$$\sigma_{j22} = \sigma_{j33} = \sigma_{j23} = 0 \tag{18}$$

$$\epsilon_{j22} = \epsilon_{j33} = \epsilon_{j23} = 0 \tag{19}$$

$$\sigma_{j11} = E_j \epsilon_{j11} \tag{20}$$

$$\sigma_{j12} = G_j \epsilon_{j12} \tag{21}$$

$$\sigma_{j13} = G_j \epsilon_{j13} \tag{22}$$

where E_j is the Young modulus of body j and G_j is its shear modulus.

Introducing Eqs. (16*a*)–(22) into Eqs. (8) and (15) for $\mathbf{q}_{\mathrm{e}_j} = \mathbf{0}$, the stiffness matrix of body j takes the form

$$\mathbf{K}_j = \frac{1}{l_j^3} \begin{bmatrix} E_j A_j l_j^2 & 0 & 0 & 0 & 0 & 0 \\ 0 & 12E_j I_{z_j} & 0 & 0 & 0 & -6E_j I_{z_j} l_j \\ 0 & 0 & 12E_j I_{y_j} & 0 & 6E_j I_{y_j} l_j & 0 \\ 0 & 0 & 0 & I_{0_j} G_j l_j^2 & 0 & 0 \\ 0 & 0 & 6E_j I_{y_j} l_j & 0 & 4E_j I_{y_j} l_j^2 & 0 \\ 0 & -6E_j I_{z_j} l_j & 0 & 0 & 0 & 4E_j I_{z_j} l_j^2 \end{bmatrix} \tag{23}$$

where A_j is the beam cross section area, I_{y_j}, and I_{z_j} are the second moments of area around axes y and z of the local frame, I_{0_j} is the torsion constant.

Similarly, the mass matrix of body j is expressed as

$$\mathbf{M}_j = \begin{bmatrix} \mathbf{M}_{11_j} & \mathbf{M}_{12_j} \\ \mathbf{M}_{12_j}^{\mathrm{T}} & \mathbf{M}_{22_j} \end{bmatrix} \tag{24}$$

where

$$\mathbf{M}_{11_j} = \begin{bmatrix} m_j & 0 & 0 & 0 & m_j z_{G_j} & -m_j y_{G_j} \\ 0 & m_j & 0 & -m_j z_{G_j} & 0 & m_j x_{G_j} \\ 0 & 0 & m_j & m_j y_{G_j} & -m_j x_{G_j} & 0 \\ 0 & -m_j z_{G_j} & m_j y_{G_j} & J_{xx_j} & J_{xy_j} & J_{xz_j} \\ m_j z_{G_j} & 0 & -m_j x_{G_j} & J_{xy_j} & J_{yy_j} & J_{yz_j} \\ -m_j y_{G_j} & m_j x_{G_j} & 0 & J_{xz_j} & J_{yz_j} & J_{zz_j} \end{bmatrix} \tag{25}$$

$$\mathbf{M}_{12_j} = \begin{bmatrix} \frac{m_j}{2} & 0 & 0 & 0 & 0 & 0 \\ 0 & \frac{m_j}{2} & 0 & 0 & 0 & \frac{m_j l_j}{12} \\ 0 & 0 & \frac{m_j}{2} & 0 & \frac{m_j l_j}{12} & 0 \\ 0 & 0 & 0 & \frac{\rho_j l_j I_{\mathrm{p}_j}}{2} & 0 & 0 \\ 0 & 0 & -\rho_j I_{y_j} - \frac{7m_j l_j}{20} & 0 & -\frac{m_j l_j^2}{20} & 0 \\ 0 & \rho_j I_{z_j} + \frac{7m_j l_j}{20} & 0 & 0 & 0 & -\frac{m_j l_j^2}{20} \end{bmatrix} \tag{26}$$

$$\mathbf{M}_{22_j} = \begin{bmatrix} \frac{m_j}{3} & 0 & 0 & 0 & 0 & 0 \\ 0 & \frac{13m_j}{35} + \frac{6\rho_j I_{z_j}}{5l_j} & 0 & 0 & 0 & -\frac{11m_j l_j + 21\rho_j I_{z_j}}{210} \\ 0 & 0 & \frac{13m_j}{35} + \frac{6\rho_j I_{y_j}}{5l_j} & 0 & \frac{11m_j l_j + 21\rho_j I_{y_j}}{210} & 0 \\ 0 & 0 & 0 & \frac{\rho_j l_j I_{\mathrm{p}_j}}{3} & 0 & 0 \\ 0 & 0 & \frac{11m_j l_j + 21\rho_j I_{y_j}}{210} & 0 & \frac{m_j l_j^2 + 14\rho_j I_{y_j} l_j}{105} & 0 \\ 0 & -\frac{11m_j l_j + 21\rho_j I_{z_j}}{210} & 0 & 0 & 0 & \frac{m_j l_j^2 + 14\rho_j I_{z_j} l_j}{105} \end{bmatrix} \tag{27}$$

and

- x_{G_j}, y_{G_j}, and z_{G_j} are the Cartesian coordinates of the center of mass of body j expressed in frame $\mathcal{F}_j$;
- $J_{xx_j}, J_{yy_j}, J_{zz_j}, J_{xy_j}, J_{xz_j}$, and J_{yz_j} are the terms of the rigid inertia matrix expressed at the origin of frame $\mathcal{F}_j$;
- $I_{p_j} = I_{y_j} + I_{z_j}$ is the polar moment of inertia.

3 Computation of the Stiffness and Mass Matrices of a Tree Structure Robot

Let us consider a parallel robot composed of one rigid fixed base (denoted as element 0), one rigid moving platform and n legs, each leg being a serial kinematic chain composed of $m_i - 1$ elements[2] connected by m_i joints (revolute, prismatic or fixed joints $- i = 1,\ldots, n$) located at points C_{ik} ($k = 1,\ldots, m_i$—Fig. 1(*a*)). The jth element of the ith leg is denoted by ij. The nominal values of the actuated variables (of the passive variables, resp.) are denoted by $\mathbf{q}_a$ ($\mathbf{q}_p$, resp.). The nominal values of the Cartesian coordinates of the platform are denoted by $\mathbf{x}_p$. The dimension n_a of vector $\mathbf{q}_a$ must be greater than or equal to the number of degrees of freedom of the parallel robot. Under the assumption of an elastic deformation, the variations in those variables are denoted by $\delta\mathbf{q}_a$, $\delta\mathbf{q}_p$, and $\delta\mathbf{x}_p$, respectively.

The number of shape functions for the element ij is denoted by N_{ij} ($j = 1,\ldots, m_i - 1$). As a result, the dimension n_e of the vector of elastic variables $\mathbf{q}_e$ is equal to $\sum_{i=1}^{n}\sum_{j=1}^{m_i-1} N_{ij}$.

Thus, the vector of generalized coordinates of the tree-structure is given by $\mathbf{q}_t = \left[\mathbf{q}_{t_1}^T \cdots \mathbf{q}_{t_n}^T\right]^T$, where $\mathbf{q}_{t_i} = \left[\delta\mathbf{q}_{a_i}^T \;\; \delta\mathbf{q}_{p_i}^T \;\; \mathbf{q}_{e_i}^T\right]^T$. $\delta\mathbf{q}_{a_i}, \delta\mathbf{q}_{p_i}$, and $\mathbf{q}_{e_i}$ are the vectors of the actuated, passive, and elastic generalized coordinates for the ith leg.

3.1 Relationships Between the Generalized Coordinates of a Flexible Body and the Generalized Coordinates of the Tree Structure.

The generalized velocities $\mathbf{v}_{ij}(A_{ij}), \boldsymbol{\omega}_{ij}(A_{ij})$, and $\dot{\mathbf{q}}_{e_{ij}}$ of body ij are linked to the generalized velocities[3] $\dot{\mathbf{q}}_t$ by the relations

$$\begin{bmatrix} \mathbf{v}_{ij}(A_{ij}) \\ \boldsymbol{\omega}_{ij}(A_{ij}) \end{bmatrix} = \mathbf{J}_{v_{ij}}^{i}\dot{\mathbf{q}}_{t_i} = \mathbf{J}_{v_{ij}}\dot{\mathbf{q}}_t \tag{28}$$

with

$$\mathbf{J}_{v_{ij}} = \begin{bmatrix} \mathbf{0} & \cdots & \mathbf{J}_{v_{ij}}^{i} & \cdots & \mathbf{0} \end{bmatrix} \tag{29a}$$

$$\dot{\mathbf{q}}_t = \begin{bmatrix} \dot{\mathbf{q}}_{t_1} \\ \vdots \\ \dot{\mathbf{q}}_{t_i} \\ \vdots \\ \dot{\mathbf{q}}_{t_n} \end{bmatrix} \tag{29b}$$

and

$$\dot{\mathbf{q}}_{e_{ij}} = \mathbf{J}_{e_{ij}}\dot{\mathbf{q}}_t \tag{30}$$

The foregoing equations can be rewritten in the following compact form:

$$\begin{bmatrix} \mathbf{v}_{ij}(A_{ij}) \\ \boldsymbol{\omega}_{ij}(A_{ij}) \\ \dot{\mathbf{q}}_{e_{ij}} \end{bmatrix} = \mathbf{J}_{ij}\dot{\mathbf{q}}_t \tag{31}$$

with

$$\mathbf{J}_{ij} = \begin{bmatrix} \mathbf{J}_{v_{ij}} \\ \mathbf{J}_{e_{ij}} \end{bmatrix} \tag{32}$$

$\mathbf{J}_{ij}$ is the Jacobian matrix mapping the generalized velocities $\dot{\mathbf{q}}_t$ of the tree structure into the generalized velocities of the element ij. $\mathbf{J}_{v_{ij}}$ is the Jacobian matrix mapping $\dot{\mathbf{q}}_t$ into the twist of the local frame attached to element ij. $\mathbf{J}_{e_{ij}}$ is a matrix composed of 0 and 1 terms that is used to extract vector $\dot{\mathbf{q}}_{e_{ij}}$ from vector $\dot{\mathbf{q}}_t$.

Matrix $\mathbf{J}_{v_{ij}}$ is expressed thanks to a generic and systematic approach described thereafter and derived from Ref. [22].

Let us first compute the homogeneous transformation matrix $\mathbf{T}_{ij}$ that defines the location and orientation of the local frame attached to the element ij. By definition, this element is located in the leg i and is preceded by $j-1$ elements, each element ik ($k = 1,\ldots,j$) being linked to another by a joint (revolute, prismatic or fixed) described by its nominal coordinate q_{ik} (Fig. 1(*b*)). Thus, matrix $\mathbf{T}_{ij}$ is defined by

$$\mathbf{T}_{ij} = \mathbf{T}_{\text{base}}^{i}\left(\prod_{k=1}^{j-1}\left(\mathbf{V}_a(q_{ik})\mathbf{T}_{\text{elt}}^{ik}\mathbf{V}_e(\mathbf{q}_{e_{ik}})\right)\right)\mathbf{V}_a(q_{ij})\mathbf{T}_{\text{end}}^{ij} \tag{33}$$

where

- $\mathbf{T}_{\text{base}}^{i}$ denotes the rigid transformation between the global base frame and the frame attached to ith leg;
- The matrix function $\mathbf{V}_a(.)$ is a transformation matrix corresponding to an elementary rotation or an elementary translation;
- $\mathbf{T}_{\text{elt}}^{ik}$ denotes the rigid transformation matrix between the frame attached to element ik and the frame attached to element $i, k+1$ in the undeformed case;
- The matrix function $\mathbf{V}_e(.)$ represents the translations and rotations due to the deformations of the flexible link (if the element is rigid, this matrix will be the identity matrix $\mathbf{q}_{e_{ik}} = \mathbf{0}$ in this case);
- $\mathbf{T}_{\text{end}}^{ij}$ is a matrix that allows the rotational part of $\mathbf{T}_{ij}$ to be equal to the identity matrix.

Then, let us gather all variables introduced in Eq. (33) into vector

$$\mathbf{q}_{t_{ij}} = \left[q_{i1}\mathbf{q}_{e_{i1}}^T \cdots \mathbf{q}_{e_{i,j-1}}^T q_{ij}\right]^T \tag{34}$$

and assume that for the lth variable $q_{t_{ijl}}$ of vector $\mathbf{q}_{t_{ij}}$, Eq. (33) is rewritten as

$$\mathbf{T}_{ij} = \mathbf{H}_{ijl}^{R}\mathbf{V}_{ijl}(q_{t_{ijl}})\mathbf{H}_{ijl}^{L} \tag{35}$$

where the first and the third multipliers are constant homogeneous matrices while the second multiplier is either an elementary translation matrix or an elementary rotation matrix. Then the partial derivative of the homogeneous matrix $\mathbf{T}_{ij}$ with respect to $q_{t_{ijl}}$ at the configuration $q_{t_{ijl}}^{\text{nom}}$ ($q_{t_{ijl}}^{\text{nom}} = 0$ for an elastic variable and may not vanish for a joint variable) can be computed from a similar product where the internal term is replaced by the matrix $\mathbf{V}_{ijl}^{d}(.) = \partial\mathbf{V}_{ijl}(q_{t_{ijl}})/\partial q_{t_{ijl}}$ that takes a simple analytical form. For instance, for elementary translations and rotations along and about the x axis, these derivatives take the form

$$\mathbf{V}_{ijl}^{d}(q_{t_{ijl}}) = \begin{bmatrix} 0 & 0 & 0 & 1 \\ 0 & 0 & 0 & 0 \\ 0 & 0 & 0 & 0 \\ 0 & 0 & 0 & 0 \end{bmatrix} \text{ for a translation along } x \text{ axis}$$

$$\mathbf{V}_{ijl}^{d}(q_{t_{ijl}}) = \begin{bmatrix} 0 & 0 & 0 & 0 \\ 0 & -\sin(q_{t_{ijl}}) & -\cos(q_{t_{ijl}}) & 0 \\ 0 & \cos(q_{t_{ijl}}) & -\sin(q_{t_{ijl}}) & 0 \\ 0 & 0 & 0 & 0 \end{bmatrix}$$

for a rotation about x axis (36)

[2]Note that each robot link can be composed of one element or several elements.
[3]It is assumed that the generalized velocities are equal to $d/dt(\delta\mathbf{q}_t) = \dot{\mathbf{q}}_t$.

For the elementary translations and rotations along and about the other axes, the matrices $\mathbf{V}^{\mathrm{d}}_{ijl}(.)$ can be obtained similarly.

Only small displacements occur in the determination of the natural frequencies. Therefore, the derivative of the homogeneous matrix $\mathbf{T}^{\mathrm{d}}_{ij} = \partial \mathbf{T}_{ij}/\partial q_{\mathrm{t}_{ijl}} = \mathbf{H}^{\mathrm{R}}_{ijl}\mathbf{V}^{\mathrm{d}}_{ijl}(q_{\mathrm{t}_{ijl}})\mathbf{H}^{\mathrm{L}}_{ijl}$ can be expressed as

$$\mathbf{T}^{\mathrm{d}}_{ij} = \begin{bmatrix} 0 & -\gamma^{\mathrm{d}}_{z_{ijl}} & \gamma^{\mathrm{d}}_{y_{ijl}} & \lambda^{\mathrm{d}}_{x_{ijl}} \\ \gamma^{\mathrm{d}}_{z_{ijl}} & 0 & -\gamma^{\mathrm{d}}_{x_{ijl}} & \lambda^{\mathrm{d}}_{y_{ijl}} \\ -\gamma^{\mathrm{d}}_{y_{ijl}} & \gamma^{\mathrm{d}}_{x_{ijl}} & 0 & \lambda^{\mathrm{d}}_{z_{ijl}} \\ 0 & 0 & 0 & 0 \end{bmatrix} \tag{37}$$

It is noteworthy that vector ${}^{0}\mathbf{j}^{q_{ijl}}_{v_{ij}} = \begin{bmatrix} \lambda^{\mathrm{d}}_{x_{ijl}} & \lambda^{\mathrm{d}}_{y_{ijl}} & \lambda^{\mathrm{d}}_{z_{ijl}} & \gamma^{\mathrm{d}}_{x_{ijl}} & \gamma^{\mathrm{d}}_{y_{ijl}} & \gamma^{\mathrm{d}}_{z_{ijl}} \end{bmatrix}^{\mathrm{T}}$, which can be obtained by extracting the terms of matrix $\mathbf{T}^{\mathrm{d}}_{ij}$ defined in Eq. (37), is the column of the Jacobian matrix corresponding to variable $\dot{q}_{\mathrm{t}_{ijl}}$. The latter maps vector $\mathbf{q}_{\mathrm{t}}$ into the velocity of the local frame attached to body ij expressed in the global frame [22]. Let ${}^{ij}\overline{\mathbf{R}}_0$ be the (6×6) extended rotation matrix

$${}^{ij}\overline{\mathbf{R}}_0 = \begin{bmatrix} {}^{ij}\mathbf{R}_0 & \mathbf{0}_3 \\ \mathbf{0}_3 & {}^{ij}\mathbf{R}_0 \end{bmatrix} \tag{38}$$

where ${}^{ij}\mathbf{R}_0$ is the rotation matrix between the global frame and the local frame attached to element ij, which is evaluated in the robot undeformed configuration and can be extracted using Eq. (33). Thus, multiplying ${}^{ij}\overline{\mathbf{R}}_0$ by vector ${}^{0}\mathbf{j}^{q_{ijl}}_{v_{ij}}$ yields the column $\mathbf{j}^{q_{ijl}}_{v_{ij}} = {}^{ij}\overline{\mathbf{R}}^{0}_{0}\mathbf{j}^{q_{ijl}}_{v_{ij}}$ of Jacobian matrix $\mathbf{J}_{v_{ij}}$ defined in Eq. (28) corresponding to variable $\dot{q}_{\mathrm{t}_{ijl}}$.

3.2 Stiffness and Mass Matrices of the Tree Structure. From Eqs. (6) and (9), the Lagrangian of the tree structure system can be expressed as

$$\begin{aligned} L_{\mathrm{t}} &= \sum_{i,j} \left(T_{ij} - V_{\mathrm{e}_{ij}}\right) \\ &= \frac{1}{2}\sum_{i,j} \left(\begin{bmatrix} \mathbf{v}_{ij}(A_{ij}) \\ \boldsymbol{\omega}_{ij}(A_{ij}) \\ \dot{\mathbf{q}}_{\mathrm{e}_{ij}} \end{bmatrix}^{\mathrm{T}} \mathbf{M}_{ij} \begin{bmatrix} \mathbf{v}_{ij}(A_{ij}) \\ \boldsymbol{\omega}_{ij}(A_{ij}) \\ \dot{\mathbf{q}}_{\mathrm{e}_{ij}} \end{bmatrix} - \mathbf{q}^{\mathrm{T}}_{\mathrm{e}_{ij}}\mathbf{K}_{ij}\mathbf{q}_{\mathrm{e}_{ij}} \right) \end{aligned} \tag{39}$$

Introducing Eq. (28) into Eq. (39) leads to

$$\begin{aligned} L_{\mathrm{t}} &= \frac{1}{2}\sum_{i,j} \left(\dot{\mathbf{q}}^{\mathrm{T}}_{\mathrm{t}}\mathbf{J}^{\mathrm{T}}_{ij}\mathbf{M}_{ij}\mathbf{J}_{ij}\dot{\mathbf{q}}_{\mathrm{t}} - \mathbf{q}^{\mathrm{T}}_{\mathrm{t}}\mathbf{J}^{\mathrm{T}}_{\mathrm{e}_{ij}}\mathbf{K}_{ij}\mathbf{J}_{\mathrm{e}_{ij}}\mathbf{q}_{\mathrm{t}} \right) \\ &= \frac{1}{2}\left(\dot{\mathbf{q}}^{\mathrm{T}}_{\mathrm{t}}\mathbf{M}_{\mathrm{t}}\dot{\mathbf{q}}_{\mathrm{t}} - \mathbf{q}^{\mathrm{T}}_{\mathrm{t}}\mathbf{K}_{\mathrm{t}}\mathbf{q}_{\mathrm{t}} \right) \end{aligned} \tag{40}$$

where $\mathbf{M}_{\mathrm{t}}$ and $\mathbf{K}_{\mathrm{t}}$ are the mass and stiffness matrices of the tree structure.

Adding the contribution of the rigid platform into Eq. (40), the Lagrangian of the total system can be written as

$$\begin{aligned} L &= \frac{1}{2}\left(\dot{\mathbf{q}}^{\mathrm{T}}_{\mathrm{t}}\mathbf{M}_{\mathrm{t}}\dot{\mathbf{q}}_{\mathrm{t}} + \dot{\mathbf{x}}^{\mathrm{T}}_{\mathrm{p}}\mathbf{M}_{\mathrm{p}}\dot{\mathbf{x}}_{\mathrm{p}} - \mathbf{q}^{\mathrm{T}}_{\mathrm{t}}\mathbf{K}_{\mathrm{t}}\mathbf{q}_{\mathrm{t}} \right) \\ &= \frac{1}{2}\left(\begin{bmatrix} \dot{\mathbf{q}}^{\mathrm{T}}_{\mathrm{t}} & \dot{\mathbf{x}}^{\mathrm{T}}_{\mathrm{p}} \end{bmatrix} \begin{bmatrix} \mathbf{M}_{\mathrm{t}} & \mathbf{0} \\ \mathbf{0} & \mathbf{M}_{\mathrm{p}} \end{bmatrix} \begin{bmatrix} \dot{\mathbf{q}}_{\mathrm{t}} \\ \dot{\mathbf{x}}_{\mathrm{p}} \end{bmatrix} - \begin{bmatrix} \mathbf{q}^{\mathrm{T}}_{\mathrm{t}} & \delta\mathbf{x}^{\mathrm{T}}_{\mathrm{p}} \end{bmatrix} \begin{bmatrix} \mathbf{K}_{\mathrm{t}} & \mathbf{0} \\ \mathbf{0} & \mathbf{0} \end{bmatrix} \begin{bmatrix} \mathbf{q}_{\mathrm{t}} \\ \delta\mathbf{x}_{\mathrm{p}} \end{bmatrix} \right) \\ &= \frac{1}{2}\left(\dot{\mathbf{q}}^{\mathrm{T}}_{\mathrm{tot}}\mathbf{M}_{\mathrm{tot}}\dot{\mathbf{q}}_{\mathrm{tot}} - \mathbf{q}^{\mathrm{T}}_{\mathrm{tot}}\mathbf{K}_{\mathrm{tot}}\mathbf{q}_{\mathrm{tot}} \right) \end{aligned} \tag{41}$$

where $\mathbf{M}_{\mathrm{p}}$ is the mass matrix of the rigid platform. $\mathbf{M}_{\mathrm{tot}}$ and $\mathbf{K}_{\mathrm{tot}}$ are the total mass and stiffness matrices of the virtual system. $\mathbf{q}_{\mathrm{tot}} = \begin{bmatrix} \mathbf{q}^{\mathrm{T}}_{\mathrm{t}} & \delta\mathbf{x}^{\mathrm{T}}_{\mathrm{p}} \end{bmatrix}^{\mathrm{T}}$ is the vector of all generalized coordinates of the virtual system.

4 Computation of the Stiffness and Mass Matrices of the Parallel Robot

The model of the virtual tree structure and of the free moving platform does not consider the closed-loop kinematic chains. As a matter of fact, the $n_{q_{\mathrm{tot}}}$ components of vector $\mathbf{q}_{\mathrm{tot}}$ are dependent. The independent components are gathered into vector $\mathbf{q}$ and their determination is described thereafter.

4.1 Determination of the Generalized Coordinates of the Parallel Robot. For determining one possible subset of generalized coordinates for the parallel robot, let us express the relations between the vector of generalized velocities $\dot{\mathbf{q}}_{\mathrm{t}_i}$ and the twist of the last element m_i for each leg i. Using Eq. (28) for computing the twist[4] $\mathbf{t}_{i,m_i} = \begin{bmatrix} \mathbf{v}^{\mathrm{T}}_{i,m_i}(A_{i,m_i}) & \boldsymbol{\omega}^{\mathrm{T}}_{i,m_i}(A_{i,m_i}) \end{bmatrix}^{\mathrm{T}}$ of the extremity of each leg, it comes

$$\mathbf{t}_{i,m_i} = \mathbf{J}^{i}_{v_{i,m_i}}\dot{\mathbf{q}}_{\mathrm{t}_i} \tag{42}$$

As the leg extremity is also linked to the rigid platform, its twist can be related to the platform twist $\dot{\mathbf{x}}_{\mathrm{p}}$ via the rigid body displacement relation

$$\mathbf{t}_{i,m_i} = \mathbf{J}^{i}_{\mathrm{p}}\dot{\mathbf{x}}_{\mathrm{p}} \tag{43}$$

where

$$\mathbf{J}^{i}_{\mathrm{p}} = {}^{i,m_i}\overline{\mathbf{R}}_0 \begin{bmatrix} \mathbf{I}_3 & [\mathbf{p}_i]_{\times} \\ \mathbf{0} & \mathbf{I}_3 \end{bmatrix} \tag{44}$$

in which $\mathbf{J}^{i}_{\mathrm{p}}$ is a (6×6) matrix, $[\mathbf{p}_i]_{\times}$ is the cross product matrix of vector $\mathbf{p}_i$ that characterizes the position of the attachment point C_{i,m_i} with respect to the platform centre position (Fig. 1(*a*)) and ${}^{i,m_i}\overline{\mathbf{R}}_0$ is the (6×6) rotation matrix between the global frame and the local frame attached to element i, m_i, evaluated in the robot undeformed configuration.

Thus, expressing the twist $\mathbf{t}_{i,m_i}$ for each leg as a function of the platform twist $\dot{\mathbf{x}}_{\mathrm{p}}$ and generalized coordinates $\dot{\mathbf{q}}_{\mathrm{t}_i}$, the following set of equations is obtained:

$$\begin{bmatrix} \mathbf{J}^{1}_{v_{1,m_1}} & \cdots & \mathbf{0} \\ \vdots & \ddots & \vdots \\ \mathbf{0} & \cdots & \mathbf{J}^{n}_{v_{n,m_n}} \end{bmatrix} \begin{bmatrix} \dot{\mathbf{q}}_{\mathrm{t}_1} \\ \vdots \\ \dot{\mathbf{q}}_{\mathrm{t}_n} \end{bmatrix} - \begin{bmatrix} \mathbf{J}^{1}_{\mathrm{p}} \\ \vdots \\ \mathbf{J}^{n}_{\mathrm{p}} \end{bmatrix} \dot{\mathbf{x}}_{\mathrm{p}} = \mathbf{0} \tag{45}$$

which can be equivalently written as

$$\mathbf{J}_v\dot{\mathbf{q}}_{\mathrm{t}} - \mathbf{J}_{\mathrm{p}}\dot{\mathbf{x}}_{\mathrm{p}} = \begin{bmatrix} \mathbf{J}_v & -\mathbf{J}_{\mathrm{p}} \end{bmatrix} \begin{bmatrix} \dot{\mathbf{q}}_{\mathrm{t}} \\ \dot{\mathbf{x}}_{\mathrm{p}} \end{bmatrix} = \mathbf{J}_{\mathrm{tot}}\dot{\mathbf{q}}_{\mathrm{tot}} = \mathbf{0} \tag{46}$$

where $\mathbf{J}_{\mathrm{tot}}$ is a $(rn \times n_{q\mathrm{tot}})$ matrix in the case of a spatial robot, $n_{q_{\mathrm{tot}}} > rn$ ($r = 6$ for a spatial robot, $r = 3$ for a planar robot). This means that a subset $\mathbf{q}_{\mathrm{d}}$ of rn variables in vector $\mathbf{q}_{\mathrm{tot}}$ is linked to the others. This subset is not unique. An idea could be to put in this subset all passive joints and platform variables, i.e., $\mathbf{q}^{*}_{\mathrm{d}} = \begin{bmatrix} \delta\mathbf{q}^{\mathrm{T}}_{\mathrm{p}} & \delta\mathbf{x}_{\mathrm{p}} \end{bmatrix}$. However, for overconstrained parallel robots, $\dim(\mathbf{q}^{*}_{\mathrm{d}}) < r\ n$. As a result, this vector should be completed using some other elastic variables that could be chosen arbitrarily. Meanwhile, most parallel robots have identical legs and such a

[4]Note that index ij is written i, j in this section for a better understanding of the equations.

methodology will lead to an asymmetrical description of the leg variables, which is not ideal. In order to avoid this problem, we had better put in $\mathbf{q}_\mathrm{d}$ the last r components $\mathbf{q}^\mathrm{f}_{\mathrm{t}_i}$ of each vector $\mathbf{q}_{\mathrm{t}_i}$ that is now decomposed into two parts: $\mathbf{q}_{\mathrm{t}_i} = \left[\mathbf{q}^{0\mathrm{T}}_{\mathrm{t}_i}\ \mathbf{q}^{\mathrm{fT}}_{\mathrm{t}_i}\right]^\mathrm{T}$. Thus, variables $\mathbf{q}^\mathrm{f}_{\mathrm{t}_i}$ are related to the others using Eq. (45)

$$-\begin{bmatrix} \mathbf{J}^{\mathrm{f}1}_{v_{1,m_1}} & \cdots & \mathbf{0} \\ \vdots & \ddots & \vdots \\ \mathbf{0} & \cdots & \mathbf{J}^{\mathrm{f}n}_{v_{n,m_n}} \end{bmatrix} \begin{bmatrix} \dot{\mathbf{q}}^\mathrm{f}_{\mathrm{t}_1} \\ \vdots \\ \dot{\mathbf{q}}^\mathrm{f}_{\mathrm{t}_n} \end{bmatrix} = \begin{bmatrix} \mathbf{J}^{01}_{v_{1,m_1}} & \cdots & \mathbf{0} & -\mathbf{J}^1_\mathrm{p} \\ \vdots & \ddots & \vdots & \vdots \\ \mathbf{0} & \cdots & \mathbf{J}^{0n}_{v_{n,m_n}} & -\mathbf{J}^n_\mathrm{p} \end{bmatrix} \begin{bmatrix} \dot{\mathbf{q}}^0_{\mathrm{t}_1} \\ \vdots \\ \dot{\mathbf{q}}^0_{\mathrm{t}_n} \\ \dot{\mathbf{x}}_\mathrm{p} \end{bmatrix} \tag{47}$$

which can be rewritten as

$$-\mathbf{J}^\mathrm{f}_v \begin{bmatrix} \dot{\mathbf{q}}^\mathrm{f}_{\mathrm{t}_1} \\ \vdots \\ \dot{\mathbf{q}}^\mathrm{f}_{\mathrm{t}_n} \end{bmatrix} = \begin{bmatrix} \mathbf{J}^0_v & -\mathbf{J}_\mathrm{p} \end{bmatrix} \begin{bmatrix} \dot{\mathbf{q}}^0_{\mathrm{t}_1} \\ \vdots \\ \dot{\mathbf{q}}^0_{\mathrm{t}_n} \\ \dot{\mathbf{x}}_\mathrm{p} \end{bmatrix} \tag{48}$$

or also

$$\begin{aligned} \begin{bmatrix} \dot{\mathbf{q}}^\mathrm{f}_{\mathrm{t}_1} \\ \vdots \\ \dot{\mathbf{q}}^\mathrm{f}_{\mathrm{t}_n} \end{bmatrix} &= -\left(\mathbf{J}^\mathrm{f}_v\right)^{-1} \begin{bmatrix} \mathbf{J}^0_v & -\mathbf{J}_\mathrm{p} \end{bmatrix} \begin{bmatrix} \dot{\mathbf{q}}^0_{\mathrm{t}_1} \\ \vdots \\ \dot{\mathbf{q}}^0_{\mathrm{t}_n} \\ \dot{\mathbf{x}}_\mathrm{p} \end{bmatrix} \\ &= \begin{bmatrix} \mathbf{J}_{\mathrm{d}_{1,1}} & \cdots & \mathbf{J}_{\mathrm{d}_{1,n}} & \mathbf{J}_{\mathrm{d}_{1,n+1}} \\ \vdots & \ddots & \vdots & \vdots \\ \mathbf{J}_{\mathrm{d}_{n,1}} & \cdots & \mathbf{J}_{\mathrm{d}_{n,n}} & \mathbf{J}_{\mathrm{d}_{n,n+1}} \end{bmatrix} \dot{\mathbf{q}} \end{aligned} \tag{49}$$

where

- $\mathbf{J}^{0i}_{v_{i,m_i}}$ ($\mathbf{J}^{fi}_{v_{i,m_i}}$, resp.) collects the columns of matrix $\mathbf{J}^i_{v_{i,m_i}}$ corresponding to variables $\dot{\mathbf{q}}^0_{\mathrm{t}_i}$ ($\dot{\mathbf{q}}^\mathrm{f}_{\mathrm{t}_i}$, resp.);
- $\mathbf{J}_{\mathrm{d}_{ij}}$ is the matrix that maps $\dot{\mathbf{q}}^0_{\mathrm{t}_j}$ into $\dot{\mathbf{q}}^\mathrm{f}_{\mathrm{t}_i}, j = 1, \ldots, n$;
- $\mathbf{J}_{\mathrm{d}_{i,n+1}}$ is the matrix that maps $\dot{\mathbf{x}}_\mathrm{p}$ into $\dot{\mathbf{q}}^\mathrm{f}_{\mathrm{t}_i}$.

It is noteworthy that the inversion of matrix $\mathbf{J}^\mathrm{f}_v$ involves only the inversion of the $(r \times r)$ matrices $\mathbf{J}^{fi}_{v_{i,m_i}}$, which is less time consuming. Moreover, when 3D beam elements are used for leg i, if the coordinates $\mathbf{q}^\mathrm{f}_{\mathrm{t}_i}$ are the elastic coordinates the lth element of this leg (previously denoted as $\mathbf{q}_{\mathrm{e}i,l}$), it can be proven that, as the kth column of matrix $\mathbf{J}^{fi}_{v_{il}}$ corresponds to a unit twist that describes the displacement of the leg extremity due to the kth coordinate of vector $\mathbf{q}^\mathrm{f}_{\mathrm{t}_i}$, $\mathbf{J}^{fi}_{v_{il}}$ is equal to [23]

$$\mathbf{J}^{fi}_{v_{il}} = \begin{bmatrix} {}^{i,m_i}\mathbf{R}_{il} & {}^{i,m_i}\mathbf{R}_{il}\,[\mathbf{p}_{il}]_\times \\ \mathbf{0} & {}^{i,m_i}\mathbf{R}_{il} \end{bmatrix} \tag{50}$$

where ${}^{i,m_i}\mathbf{R}_{il}$ is the rotation matrix between the local frame linked at element i, m_i and the local frame linked to element il and $[\mathbf{p}_{il}]_\times$ is the cross product matrix of the vector $\mathbf{p}_{il}$ that characterizes the position of the leg extremity with respect to the frame linked to element il. Thus, its matrix inverse is equal to

$$\left(\mathbf{J}^{fi}_{v_{il}}\right)^{-1} = \begin{bmatrix} {}^{i,m_i}\mathbf{R}^\mathrm{T}_{il} & -\left([\mathbf{p}_{il}]_\times {}^{i,m_i}\mathbf{R}^\mathrm{T}_{il}\right) \\ \mathbf{0} & {}^{i,m_i}\mathbf{R}^\mathrm{T}_{il} \end{bmatrix} \tag{51}$$

which requires few calculations and, before all, avoid any numerical inversion that could lead to numerical issues. If 2D beam elements are used, some similar relations can be obtained.

Finally, the Jacobian matrix relating all variables $\dot{\mathbf{q}}_\mathrm{tot}$ to the independent variables $\dot{\mathbf{q}} = \left[\dot{\mathbf{q}}^{0\mathrm{T}}_{\mathrm{t}_1} \cdots \dot{\mathbf{q}}^{0\mathrm{T}}_{\mathrm{t}_n}\ \dot{\mathbf{x}}_\mathrm{p}\right]^\mathrm{T}$ can be obtained as

$$\dot{\mathbf{q}}_\mathrm{tot} = \begin{bmatrix} \dot{\mathbf{q}}^0_{\mathrm{t}_1} \\ \dot{\mathbf{q}}^\mathrm{f}_{\mathrm{t}_1} \\ \vdots \\ \dot{\mathbf{q}}^0_{\mathrm{t}_n} \\ \dot{\mathbf{q}}^\mathrm{f}_{\mathrm{t}_n} \\ \dot{\mathbf{x}}_\mathrm{p} \end{bmatrix} = \begin{bmatrix} \mathbf{I}_{\mathrm{c}_1} & \cdots & \mathbf{0} & \mathbf{0} \\ \mathbf{J}_{\mathrm{d}_{1,1}} & \cdots & \mathbf{J}_{\mathrm{d}_{1,n}} & \mathbf{J}_{\mathrm{d}_{1,n+1}} \\ \vdots & \cdots & \vdots & \vdots \\ \mathbf{0} & \cdots & \mathbf{I}_{\mathrm{c}_n} & \mathbf{0} \\ \mathbf{J}_{\mathrm{d}_{n,1}} & \cdots & \mathbf{J}_{\mathrm{d}_{n,n}} & \mathbf{J}_{\mathrm{d}_{n,n+1}} \\ \mathbf{0} & \cdots & \mathbf{0} & \mathbf{I}_6 \end{bmatrix} \begin{bmatrix} \dot{\mathbf{q}}^0_{\mathrm{t}_1} \\ \vdots \\ \dot{\mathbf{q}}^0_{\mathrm{t}_n} \\ \dot{\mathbf{x}}_\mathrm{p} \end{bmatrix} = \mathbf{J}\dot{\mathbf{q}} \tag{52}$$

where $\mathbf{I}_{\mathrm{c}_i}$ is the $(\mathrm{c}_i \times \mathrm{c}_i)$ identity matrix, c_i being the dimension of vector $\dot{\mathbf{q}}^0_{\mathrm{t}_i}$. Under the assumption of small displacements, the following relation holds true

$$\mathbf{q}_\mathrm{tot} = \mathbf{J}\mathbf{q} \tag{53}$$

4.2 Computation of the Natural Frequencies of the Parallel Robot. Introducing Eqs. (52) and (53) into Eq. (41) leads to

$$L = \frac{1}{2}\left(\dot{\mathbf{q}}^\mathrm{T}\mathbf{J}^\mathrm{T}\mathbf{M}_\mathrm{tot}\mathbf{J}\dot{\mathbf{q}} - \mathbf{q}^\mathrm{T}\mathbf{J}^\mathrm{T}\mathbf{K}_\mathrm{tot}\mathbf{J}\mathbf{q}\right) = \frac{1}{2}\left(\dot{\mathbf{q}}^\mathrm{T}\mathbf{M}\dot{\mathbf{q}} - \mathbf{q}^\mathrm{T}\mathbf{K}\mathbf{q}\right) \tag{54}$$

Since in the natural frequency problem, matrices $\mathbf{M}$ and $\mathbf{K}$ are evaluated in the robot nondeflected configuration, namely, for $\mathbf{q}_\mathrm{e} = 0$, and as a result for $\delta\mathbf{q}_\mathrm{a} = 0$ and $\delta\mathbf{q}_\mathrm{p} = 0$, it turns out that the Lagrange equations yield

$$\frac{d}{dt}\left(\frac{\partial L}{\partial \dot{\mathbf{q}}}\right) - \frac{\partial L}{\partial \mathbf{q}} = \mathbf{M}\ddot{\mathbf{q}} + \mathbf{K}\mathbf{q} = \mathbf{0} \tag{55}$$

A solution $\mathbf{q}_l$ of this equation satisfies

$$\left(\omega_l^2\mathbf{M} - \mathbf{K}\right)\mathbf{q}_l = \mathbf{0} \tag{56}$$

where $\omega_l = 2\pi f_l$, f_l is the natural frequency associated with the lth natural mode of vibrations and $\mathbf{q}_l$ is its associated eigenvector.

Therefore, the natural frequencies of the parallel robot are evaluated by solving the following eigenvalue problem

$$\det\left(\omega_l^2\mathbf{M} - \mathbf{K}\right) = 0 \tag{57}$$

In Sec. 5, the natural frequencies of the NaVARo, a parallel robot developed at IRCCyN [17], are computed using the proposed method and compared with the results obtained with the CAST3M software [19] and experimentally.

5 Case Study: Computation of the Natural Frequencies of the NaVaRo

5.1 Description of the NaVARo. The NaVARo was developed at IRCCyN and is shown in Fig. 3(*a*). The NaVARo is a 3DOF planar parallel manipulator composed of three identical legs and one moving platform made up of three segments E_1P, E_2P, and E_3P rigidly linked at point P. The ith leg contains four links A_iB_i, B_iC_i, C_iE_i, A_iD_i (named link $2i$, link $3i$, link $4i$, and link $1i$, respectively) connected with five revolute joints in such a way that $A_iB_iC_iD_i$ is a parallelogram linkage, $i = 1, 2, 3$. The base frame $\mathcal{F}_\mathrm{b}\left(O, \mathbf{x}_0, \mathbf{y}_0, \mathbf{z}_0\right)$ (not shown in Fig. 3(*b*)) is defined such as point O is located at the geometric centre of the equilateral triangle $A_1A_2A_3$. Frame $\mathcal{F}_\mathrm{p}\left(P, \mathbf{x}_\mathrm{p}, \mathbf{y}_\mathrm{p}, \mathbf{z}_\mathrm{p}\right)$ is attached to the moving

(a)

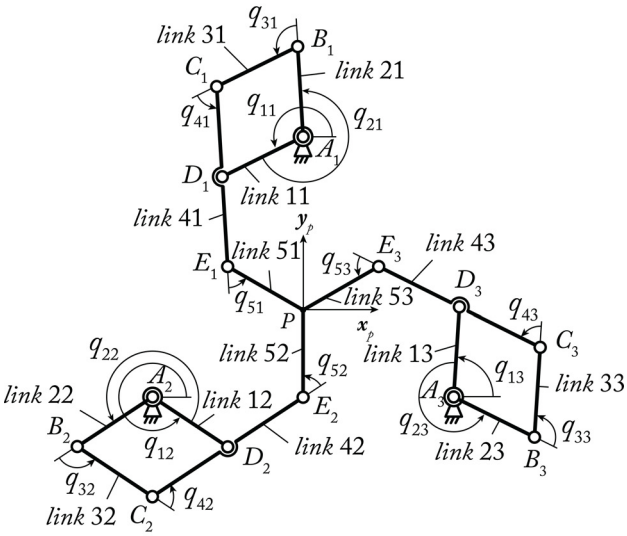

(b)

Fig. 3 The NaVARo (*a*) prototype of the NaVARo located at IRCCyN, Nantes, France and (*b*) Shematics of the NaVARo

platform. In the home configuration shown in Fig. 3, $\mathcal{F}_b$ and $\mathcal{F}_p$ coincide. (x_p, y_p) are the Cartesian coordinates of point P expressed in frame $\mathcal{F}_b$ and θ_p is the orientation angle of the moving platform, namely, the angle between $\mathbf{x}_0$ and $\mathbf{x}_p$.

Table 1 MDH parameters of the *i*th leg

ji	$a(ji)$	σ_{ji}	γ_{ji}	b_{ji}	α_{ji}	d_{ji}	θ_{ji}	r_{ji}
$1i$	0	0	γ_i	0	0	$d_1 = 0.4041$ m	q_{1i}–γ_i	0
$2i$	0	0	γ_i	0	0	$d_1 = 0.4041$ m	q_{2i}–γ_i	0
$3i$	$2i$	0	0	0	0	$d_3 = 0.2100$ m	q_{3i}	0
$4i$	$3i$	0	0	0	0	$d_4 = 0.2100$ m	q_{4i}	0
$5i$	$4i$	0	0	0	0	$d_5 = 0.4200$ m	q_{5i}	0

q_{1i} denotes the angle between axis $\mathbf{x}_0$ and link $1i$. q_{2i} denotes the angle between link $1i$ and link $2i$. Three double clutches are mounted to the base and located at points A_i, $i = 1, 2, 3$, in order to actuate either joint q_{1i} or joint q_{2i}. As a consequence, the NaVARo has eight actuation modes as described in Refs. [17] and [24]. Therefore, the moving platform can be moved throughout the manipulator workspace without reaching any parallel singularity thanks to a judicious actuation scheme.

The kinematics of the ith leg is described by the modified Denavit–Hartenberg parameters (MDH) [23] given in Table 1, in which $\gamma_i = \pi/2$ if $i = 1$, $\gamma_i = -5\pi/6$ if $i = 2$, and $\gamma_i = -\pi/6$ if $i = 3$. Besides, the circumradius of the moving-platform is equal to 0.2027 m, i.e., $l_{5i} = 0.2027$ m.

Each link, of rectangular cross section, is made up of duraluminum alloy ($E = 74000$ MPa, $G = 28900$ MPa, and $\rho = 2800$ kg/m^3). Table 2 gives the cross section area and the moments of inertia of the robot links.

In the experimental setup, the rotation of links $1i$ and $2i$ about point A_i, $i = 1, 2, 3$, is locked thanks to the double clutch mechanisms. The elasto-dynamic modeling of the NaVARo is complex due to the closed-loop chain in each leg and is obtained by following those three steps:

(1) Computation of the mass and stiffness matrices of the virtual system assuming that the moving platform is cut at point P and the parallel linkages are opened at points D_i, $i = 1, 2, 3$;
(2) Computation of the mass and stiffness matrices of the legs including the closed-loop chains;
(3) Computation of the mass and stiffness matrices of the NaVARo.

A single 3D beam element is used to model links $1i$, $2i$, $3i$, and $5i$ (see Sec. 2.4) while two 3D beam elements of equal lengths l ($l = l_{C_iD_i} = l_{D_iE_i}$) are used to model links $4i$. Links $4i$ are decomposed into two beam elements in order to close the loops as mentioned in step 2. Thus, the NaVARo is modeled as a spatial mechanism and its elasto-dynamic model contains 144 generalized coordinates: (i) 108 elastic coordinates; (ii) 12 passive joint coordinates, i.e., four passive joint angles per leg; (iii) 18 intermediary coordinates for the assembly of the legs; (iv) 6 coordinates for the moving-platform pose. From Sec. 4, it turns out that there are only 90 independent coordinates among those 144 coordinates.

5.2 Numerical Analysis. A MATLAB code was written to compute the robot mass and stiffness matrices using the modeling procedure presented in Secs. 2–4. The obtained robot mass and stiffness matrices were validated by means of an equivalent model developed using CAST3M software [19]. CAST3M aims to determine the elastodynamic model of structures modeled with beams. Both models give the same values for the first 90 natural frequencies of the NaVARo. Table 3 gives the first five natural frequencies of the NaVARo for the eight robot configurations shown in Fig. 4.

The natural frequencies of the NaVARo are the same for configurations 3, 5 and 7 (4, 6, and 8, resp.) as they correspond to a rotation of the robot base frame of ± 120 deg with respect to configuration 3 (configuration 4, resp.).

5.3 Experiments. Some experimental tests were carried out using the setup presented in Fig. 5. The application of experimental modal testing to the NaVARo was done through impact hammer

Table 2 Characteristics of the beam cross sections

link	A_{ij} (m^2)	$I_{y_{ij}}$ (m^4)	$I_{z_{ij}}$ (m^4)	$I_{p_{ij}}$ (m^4)	$I_{0_{ij}}$ (m^4)
$1i$, $2i$, $3i$, $4i$	$2.4 \cdot 10^{-4}$	$1.152 \cdot 10^{-8}$	$2.000 \cdot 10^{-9}$	$1.352 \cdot 10^{-8}$	$5.902 \cdot 10^{-9}$
$5i$	$4 \cdot 10^{-4}$	$3.333 \cdot 10^{-8}$	$5.333 \cdot 10^{-8}$	$8.666 \cdot 10^{-8}$	$1.123 \cdot 10^{-8}$

Table 3 Comparison of the natural frequencies obtained with CAST3M and the MATLAB model

(Hz)	Pose 1	Pose 2	Pose 3	Pose 4	Pose 5	Pose 6	Pose 7	Pose 8
f_1(CAST3M)	44.10	45.71	36.98	40.17	36.98	40.17	36.98	40.17
f_1(MATLAB model)	44.10	45.71	36.98	40.17	36.98	40.17	36.98	40.17
f_2(CAST3M)	44.10	45.71	49.31	50.32	49.31	50.32	49.31	50.32
f_2(MATLAB model)	44.10	45.71	49.31	50.32	49.31	50.32	49.31	50.32
f_3(CAST3M)	53.98	54.58	53.37	52.99	53.37	52.99	53.37	52.99
f_3(MATLAB model)	53.98	54.58	53.37	52.99	53.37	52.99	53.37	52.99
f_4(CAST3M)	60.63	65.35	67.28	67.36	67.28	67.36	67.28	67.36
f_4(MATLAB model)	60.63	65.35	67.28	67.36	67.28	67.36	67.28	67.36
f_5(CAST3M)	95.62	97.92	91.80	91.52	91.80	91.52	91.80	91.52
f_5(MATLAB model)	95.62	97.92	91.80	91.52	91.80	91.52	91.80	91.52

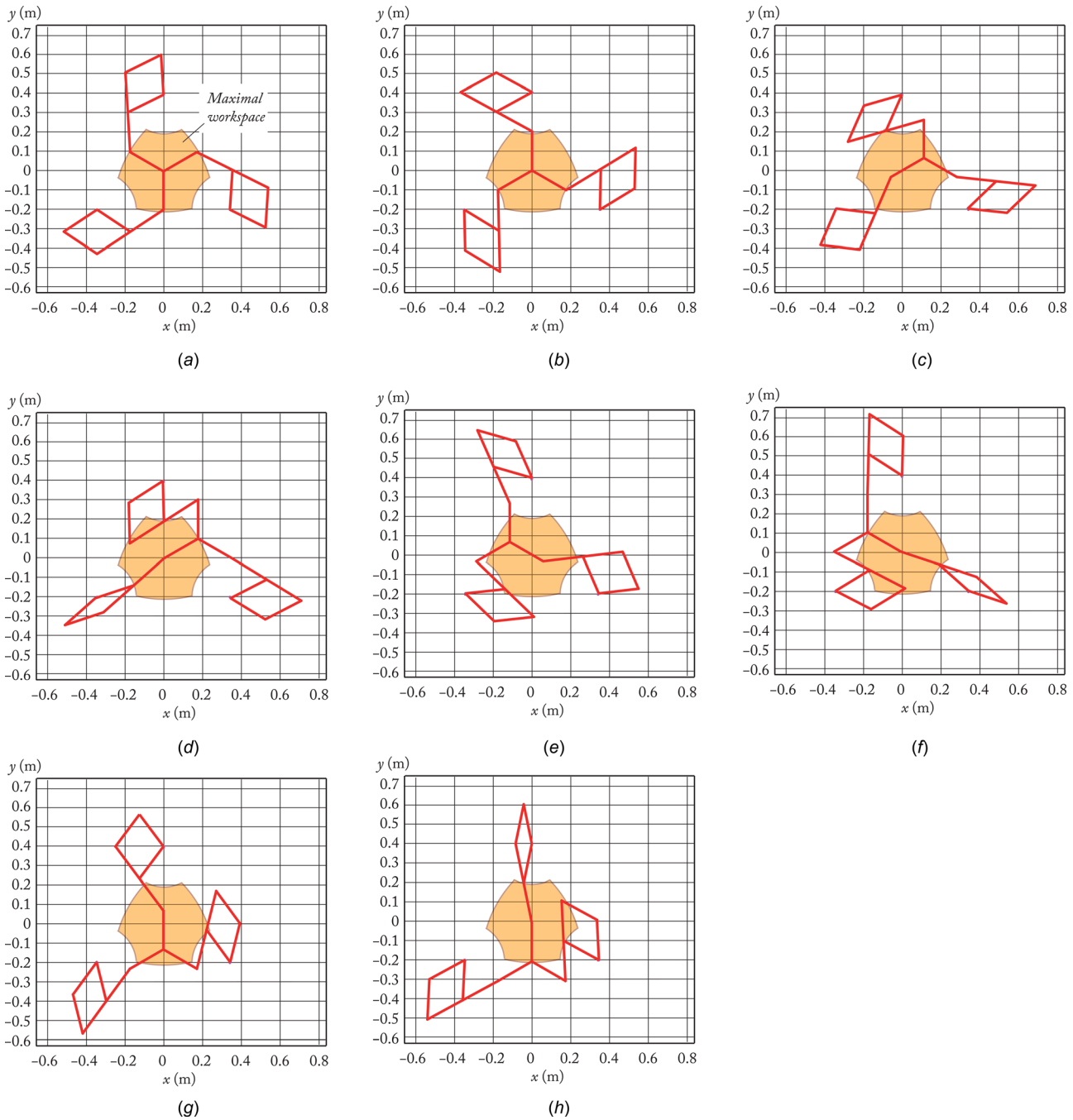

Fig. 4 The eight configurations used for the experiments: (*a*) pose 1 $x = 0$ m, $y = 0$ m, $\theta = 0$ rad; (*b*) pose 2 $x = 0$ m, $y = 0$ m, $\theta = -\pi/3$ rad; (*c*) pose 3 $x = 0.117$ m, $y = 0.068$ m, $\theta = -\pi/3$ rad; (*d*) pose 4 $x = 0.182$ m, $y = 0.105$ m, $\theta = -\pi/3$ rad;(*e*) pose 5 $x = -0.117$ m, $y = 0.068$ m, $\theta = -\pi/3$ rad; (*f*) Pose 6 $x = -0.182$ m, $y = 0.105$ m, $\theta = -\pi/3$ rad; (g) pose 7 $x = 0$ m, $y = -0.135$ m, $\theta = -\pi/3$ rad; and (*h*) pose 8 $x = 0$ m, $y = -0.21$ m, $\theta = -\pi/3$ rad

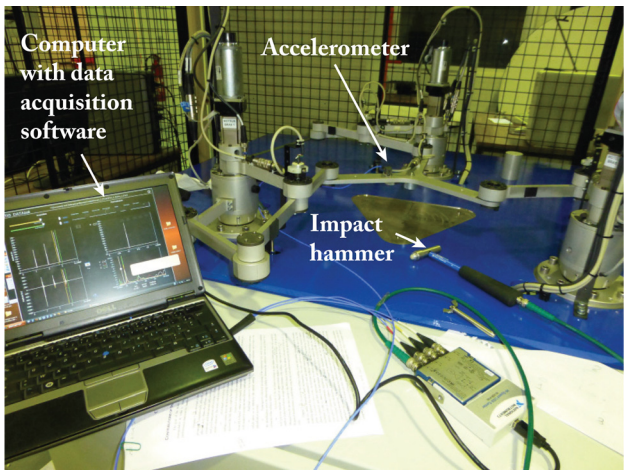

Fig. 5 Experimental setup: DATABOX

excitation, a 3D accelerometer response and data postprocessing, conducted using the DATABOX software developed at IRCCyN and sold by MITIS company. The points and directions of excitation were chosen on points B_i and E_i of each leg along all axes in order to get the maximal number of resonance frequencies. Piezoelectric triaxial accelerometers with a sensitivity of 1000 mV/g were used to pick up the three acceleration responses. The acquisitions were performed for the eight robot configurations shown in Fig. 4. Each measurement resolution is equal to 1 Hz as the acquisition time and the sampling time are equal to 1 s and 40 μs, respectively.

The resonance frequencies were obtained with a fast Fourier transform of the signals given by the triaxial accelerometer. As a result, the measured resonance frequencies between 0 and 80 Hz for configurations 1–4 are given in Table 4. As the results for configurations 3, 5, and 7 (configurations 4, 6, and 8, resp.) are similar due to the manipulator symmetry, only the results for poses 3 and 4 are given in Table 4 and the redundant configurations were used to highlight some resonance frequencies with low energy level.

It is noteworthy that the resonance frequencies of the NaVARo amount to its natural frequencies as the damping is supposed to be negligible.

Table 4 NaVARo natural frequencies (measured and computed using refined model) between 0 and 80 Hz

(Hz)	Pose 1	Pose 2	Pose 3	Pose 4
f_1 meas.	22	19	17	18
f_1 calc.	19.25	19.46	17.91	18.44
f_2 meas	24	21	19	20
f_2 calc.	20.43	20.49	19.71	19.26
f_3 meas.	32	—	23	22
f_3 calc.	40.25	41.88	20.91	21.28
f_4 meas.	—	44	27	33
f_4 calc.	43.16	45.55	—	36.88
f_5 meas.	42	45	32	43
f_5 calc.	44.10	47.05	36.88	40.60
f_6 meas.	50	53	43	44
f_6 calc.	—	—	41.86	46.13
f_7 meas.	52	54	46	50
f_7 calc.	—	56.37	45.61	55.29
f_8 meas.	62	56	48	56
f_8 calc.	67.94	—	50.52	57.81
f_9 meas.	66	60	57	58
f_9 calc.	68.81	63.10	55.45	62.27
f_{10} meas.	77	—	60	66
f_{10} calc.	79.79	—	61.04	—
f_{11} meas.	—	—	61	—
f_{11} calc.	—	—	—	—
f_{12} meas.	—	—	65	—
f_{12} calc.	—	—	65.00	—

It is apparent that the results given in Table 4 do not match with those shown in Table 3. As a matter of fact, the elasticity of the clutches has not been modeled and the joint masses have been omitted with CAST3M software as the latter cannot model lumped masses. Thus, a refined MATLAB model was written in order to consider joint masses (about 300 g per joint) and elasticities in clutches (about 2000 Nm/rad). The natural frequencies of the NaVARo computed with this refined model and the measured frequencies are gathered in Table 4 by comparing the computed mode shapes with the hammer impact direction and the direction of the vibration signals, the latter being measured by the triaxial accelerometer.

We can notice that there is a good correlation between the measured frequencies and the computed natural frequencies. Nevertheless, few predicted frequencies do not match with the measurements and vice-versa. Indeed, the theoretical and experimental results may differ due to the following reasons:

- The NaVARo has not been calibrated yet and there are some errors in the estimated moving platform pose.
- The passive joint elasticity has not been considered.
- The robot links are supposed to be coplanar in the theoretical model, whereas they are not in the prototype for collision avoidance.
- The robot links are not perfect beams as both ends are widened to insert ball bearings.
- The theoretical elastodynamic model does not consider any damping effect.

However, from those experiments, we can claim that the theoretical model is satisfactory and the proposed modeling procedure is efficient for reproducing the real behavior of any parallel robot.

6 Conclusion

Parallel robots have been increasingly used in the industry in the last few years and the characterization of their elastodynamic behavior is still an issue. Accurate elastodynamic models of parallel robots are useful at both their design and control stages in order to define their optimal dimensions and shapes while improving their vibratory behavior. Several models have been proposed in the literature. However, even if they can be adapted to any type of mechanism, they are not directly devoted to parallel manipulators and they do not provide a systematic and straightforward way for computing the Jacobian matrices associated with the kinematic constraints. Moreover, they do not take into account the symmetry in the robot leg description for choosing the independent coordinates describing the robot motion.

Therefore, a systematic method for the natural frequency computation of parallel robots has been developed in this paper. Indeed, the Jacobian matrices related to the kinematic constraints of the parallel robots are obtained in a straightforward way. Moreover, a way of choosing a symmetrical set of leg variables has been proposed. Contrary to most of the existing methods, the proposed approach does not contain any numerical matrix inversion, which is better to avoid numerical issues that may lead to a loss in the result accuracy.

This proposed approach has been used to compute the natural frequencies of the NaVARo, which is a planar parallel manipulator with multiple actuation modes developed at IRCCyN. The foregoing computed natural frequencies and those obtained with CAST3M software by using an equivalent robot model turned out to be identical. Then, some experiments have been carried out through impact hammer excitation and measurements of the platform displacements with a 3D accelerometer. The resonance frequencies obtained with a fast Fourier transform of the signals given by the triaxial accelerometer have been compared with the frequencies computed from a refined model of the robot. It appeared that there is a good correlation between the natural frequencies of the NaVARo computed with this refined model and the measured excitation frequencies.

Acknowledgment

This work has been partially funded by the French ANR project ARROW (ANR 2011 BS3 006 01). The authors would like to thank the MO2P team of IRCCyN for the impact hammer and accelerometers loan. Dr. Mathieu Ritou and Mr. Jean-Pierre Regoin are also acknowledged for their great help and good advice during the experiments on the NaVARo.

References

[1] Brogardh, T., 2007, "Present and Future Robot Control Development—An Industrial Perspective," Annu. Rev. Control, **31**(1), pp. 69–79.
[2] Chanal, H.,Duc, E., and Ray, P., 2006, "A Study of the Impact of Machine Tool Structure on Machining Processes," Int. J. Mach. Tools Manuf., **46**(2), pp. 98–106,
[3] Voglewede, P. A., and Ebert-Uphoff, I., 2005, "Overatching Framework for Measuring the Closeness to Singularities of Parallel Manipulators," IEEE Trans. Rob., **21**(6), pp. 1037–1045.
[4] Bouzgarrou, B. C., Ray, P., and Gogu, G., 2005, "New Approach for Dynamic Modelling of Flexible Manipulators," Part K: J. Multi-Body Dyn., **219**(3), pp. 285–298.
[5] Briot, S., Pashkevich, A., and Chablat, D., 2009, "On the Optimal Design of Parallel Robots Taking into Account Their Deformations and Natural Frequencies," Proceedings of the ASME 2009 International Design Engineering Technical Conferences and Computers and Information in Engineering Conference IDETC/CIE, San Diego, CA, Aug. 30–Sept. 2, pp. 367–376.
[6] Singer, N. C., and Seering, W. P., 1990, "Preshaping Command Inputs to Reduce System Vibration," ASME J. Dyn. Sys., Meas., Control, **112**(1), pp. 76–82.
[7] Singh, T., and Singhose, W. E., 2002, "Tutorial on Input Shaping/Time Delay Control of Maneuvering Flexible Structures," American Control Conference, Anchorage, AK, May 8–10, pp. 1717–1731.
[8] Pelaez, G., Pelaez, Gu., Perez, J. M., Vizan, A., and Bautista, E., 2005, "Input Shaping Reference Commands for Trajectory Following Cartesian Machines," Control Eng. Pract., **13**(8), pp. 941–958.
[9] Bouzgarrou, B. C., Fauroux, J. C., Gogu, G., and Heerah, Y., 2004, "Rigidity Analysis of t3r1 Parallel Robot Uncoupled Kinematics," Proceedings of the 35th International Symposium on Robotics, Paris, France.
[10] Bettaieb, F.,Cosson, P., and Hascoët, J.-Y., 2007, "Modeling of a High-Speed Machining Center With a Multibody Approach: The Dynamic Modeling of Flexible Manipulators," Proceedings of the 6th International Conference on High Speed Machining, San Sebastian, Spain.
[11] Shabana, A., 2005, *Dynamics of Multibody Systems*, Cambridge University Press.
[12] Rognant, M., Courteille, E., and Maurine, P., 2010, "A Systematic Procedure for the Elastodynamic Modeling and Identification of Robot Manipulators," IEEE Trans. Rob., **26**(6), pp. 1085–1093.
[13] Bauchau, O. A., 2011, *Flexible Multibody Dynamics*, Springer, Dordrecht, Heidelberg, London, New York.
[14] Cammarata, A.,Condorelli, D., and Sinatra, R., 2013, "An Algorithm to Study the Elastodynamics of Parallel Kinematic Machines With Lower Kinematic Pairs," ASME J. Mech. Rob., **5**(1), p. 011004.
[15] Wittbrodt, E., Adamiec-Wójcik, I., and Wojciech, S., 2006, *Dynamics of Flexible Multibody Systems*, Springer-Verlag, Berlin, Heidelberg, New York.
[16] Ibrahim, O., and Khalil, W., 2010, "Inverse and Direct Dynamic Models of Hybrid Robots," Mech. Mach. Theory, **45**(4), pp. 627–640.
[17] Rakotomanga, N.,Chablat, D., and Caro, S., "Kinetostatic Performance of a Planar Parallel Mechanism With Variable Actuation," *Advances in Robot Kinematics*, Springer, The Netherlands, pp. 311–320.
[18] Caro, S.,Chablat, D., Wenger, P., and Kong, X., 2014, "Kinematic and Dynamic Modeling of a Parallel Manipulator With Eight Actuation Modes," *New Trends in Medical and Service Robots*, Springer, pp. 315–329.
[19] Castem3000. The Castem Software, http:\\www-cast3m.cea.fr. Webpage accessed November 2012.
[20] Boyer, F., and Khalil, W., 1996, "Dynamics of a 3DOF Spatial Parallel Manipulator With Flexible Links," IEEE International Conference on Robotics and Automation, 1996. Proceedings of IEEE International Conference on, 1995, Nagoya, May 21–27, pp. 627–633.
[21] Blevins, R. D., 2001, "Formulas for Natural Frequency and Mode Shape," ASME J. Appl. Mech., **47**(2), pp. 461–462.
[22] Pashkevich, A., Chablat, D., and Wenger, P., 2009, "Stiffness Analysis of Overconstrained Parallel Manipulators," Mech. Mach. Theory, **44**(5), pp. 966–982.
[23] Khalil, W., and Dombre, E., 2002, *Modeling, Identification, and Control of Robots*, Hermes Penton London, London, UK.
[24] Arakelian, V., Briot, S., and Glazunov, V., 2008, "Increase of Singularity-Free Zones in the Workspace of Parallel Manipulators Using Mechanisms of Variable Structure," Mech. Mach. Theory, **43**(9), pp. 1129–1140.